Identify OH groups in TiOF2 and their impact on the lithium intercalation properties

Wei Li, Monique Body, Christophe Legein, Damien Dambournet

Identify OH groups in $TiOF_2$ and their Impact on the lithium intercalation properties

Wei Li[1], Monique Body[2], Christophe Legein[2], Damien Dambournet[1*]

[1]Sorbonne Universités, UPMC Univ Paris 06, CNRS UMR 8234 PHENIX, 75005 Paris, France.

[2]Université Bretagne Loire, Université du Maine, UMR CNRS 6283, Institut des Molécules et des Matériaux du Mans (IMMM), Avenue Olivier Messiaen, 72085 Le Mans Cedex 9, France.

[*]Corresponding author: damien.dambournet@upmc.fr

Abstract

A detailed investigation on the chemical composition of the cubic form of titanium oxyfluoride-based compound reveals the presence of OH groups substituting the oxide/ fluoride sublattice. The substitution of oxide by hydroxyl groups induces the presence of titanium vacancies (□) which were characterized by solid-state ^{1}H and ^{19}F NMR. ^{1}H NMR shows that OH groups are present as bridging Ti-OH-Ti or terminal OH groups, *i.e.* sitting close to a titanium vacancy Ti-OH-□. The electrochemical properties *vs.* Li^{+}/Li indicates that the presence of OH groups prevents the intercalation of lithium in the upper voltage region (1.2-3V *vs.* Li^{+}/Li). Indeed, a partial dehydroxylation of the framework enables to improve the reversibility of the lithium insertion/de-insertion processes. Since the presence of OH groups in this type of compounds is usual and depends on the synthesis method employed, this work enables to rationalize the different electrochemical behaviours reported in the literature and further highlights the importance of a good knowledge of the chemical composition with regard to the physico-chemical properties.

Graphical abstract

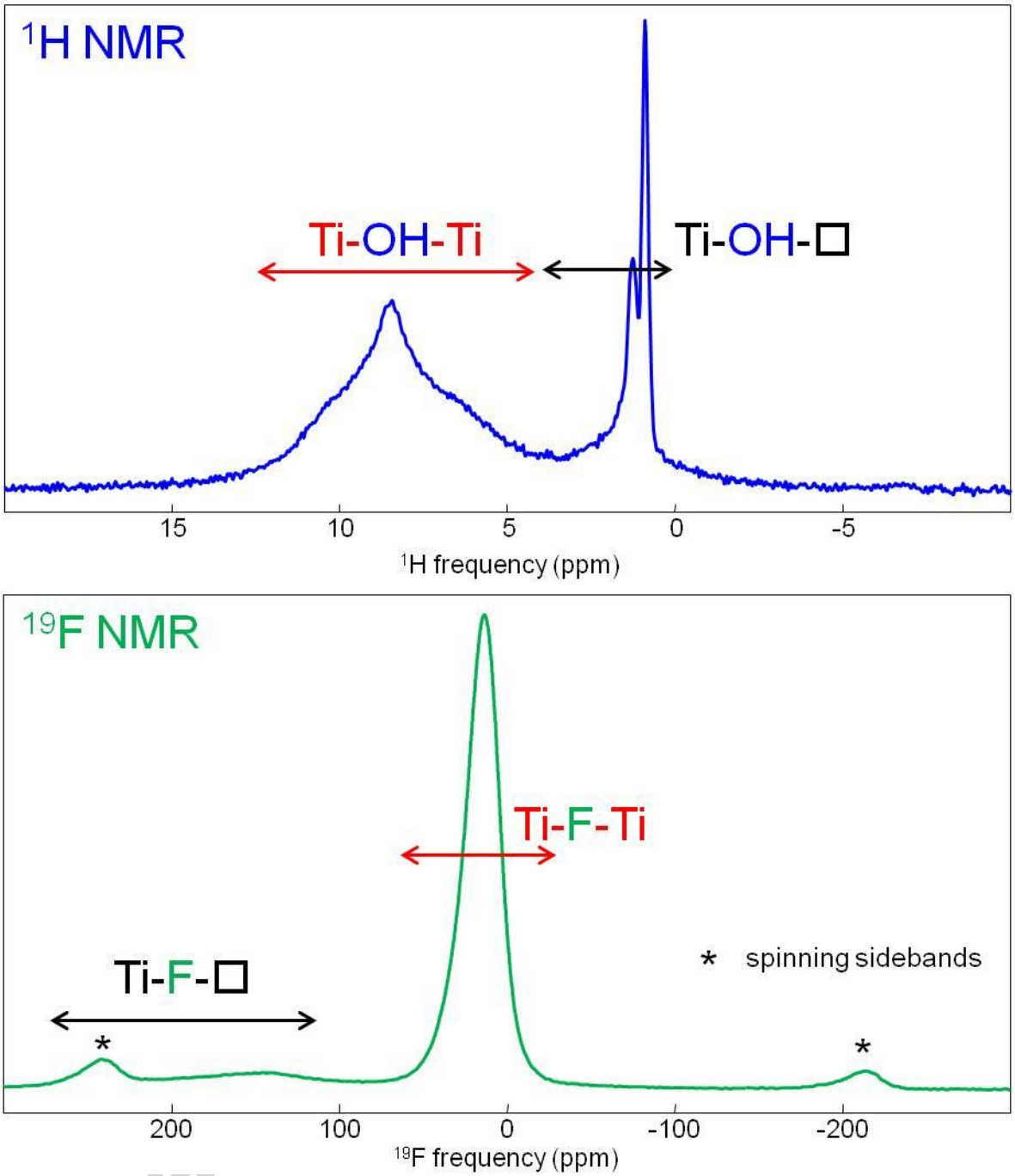

The substitution of oxide by hydroxyl groups inducing the formation of titanium vacancies (□), *i.e.*, $Ti_{1-x}□_xO_{1-4x}(OH)_{4x+y}F_{2-y}$, was characterized by solid-state ^{1}H and ^{19}F NMR.

Keywords. Titanium vacancies, transition metal oxyfluoride, ^{19}F and ^{1}H solid-state NMR, negative electrode.

Introduction

Solution-based synthesis of transition metal oxyfluoride relies on hydrolysis/fluorolysis and condensation reactions [1,2]. Accordingly, certain transition metal such as titanium or niobium can accommodate up to three types of anions, *i.e.* O^{2-}, OH^- and F^-, yielding complex compositional and structural features [3-10]. In specific conditions, the formation of oxo species can be prevented thus enabling the stabilization of hydroxyls groups. In particular, the use of acidic aqueous medium has yielded a hydroxyfluoride compound derived from $TiOF_2$. The substitution of divalent oxide by monovalent OH groups led to the formation of a significant amount of titanium vacancies, *i.e.* $Ti_{0.75}\square_{0.25}F_{1.5}(OH)_{1.5}$ [10].

Titanium oxy-(hydroxyl)-fluoride compounds have been shown to be of particular interests for a broad variety of applications spanning energy storage [11-17], optical properties [18] and photocatalysis [19-21]. The precise knowledge of the chemical composition and structural features of these compounds is of paramount importance to understand their physico-chemical properties. For instance, the lithium insertion properties of Ti-based oxyfluoride compounds in the 1.2-3 V region depend on the material's preparation methods [11-17]. In the present article, we employ a variety of analytical and spectroscopic tools to characterize OH groups in the cubic form of $TiOF_2$. Finally, we investigate how OH groups can alter the electrochemical reaction vs. Li^+/Li.

Material and methods

Synthesis.

Hydroxylated $TiOF_2$ was synthesized using a microwave-assisted solvothermal method. A solution containing 27 mmol of titanium tetraisopropoxide (TTIP, Sigma-Aldrich), 47.22 mL of isopropanol (Sigma-Aldrich) and 4.78 mL (F/Ti molar ratio of 4) of hydrofluoric acid (40 wt. %, Rectapur) was placed in a sealed Teflon line container. The solution was then heated at 90 °C for 30 min with a ramp of 13 °C/min yielding a transparent solution. The precipitation was then obtained by solvent removal using a microwave heating at 75 °C for 30 min under a nitrogen stream. The obtained powder was washed twice with ethanol. Finally, the sample was dried at 90 °C under vacuum.

Characterization methods.

X-ray diffraction was carried out by using a Rigaku Ultima IV diffractometer with a Cu Kα radiation (λ = 1.5418 Å).

The thermogravimetric analysis (TGA) was performed using Setaram Setsys. The sample was heated from room temperature up to 350 °C under a helium atmosphere (heating rate 5° C/min).

Thermal treatments of the hydroxylated $TiOF_2$ were performed in a tubular oven under vacuum for 10 hours with a heating rate of 2 °C.min^{-1}.

Solid-state NMR spectroscopy.

^1H and ^{19}F solid-state magic angle spinning (MAS) NMR experiments were performed on a Bruker Avance 300 spectrometer operating at 7.0 T (^1H and ^{19}F Larmor frequencies of 300.1 and 282.2 MHz, respectively), using a 1.3 mm CP-MAS probe head. The room temperature ^1H and ^{19}F MAS spectra were recorded using a Hahn echo sequence with an interpulse delay equal to one rotor period. The 90° pulse lengths were set to 2 μs and 1.55 μs and the recycle delays were set to 10 s and 20 s, for ^1H and ^{19}F, respectively. ^1H and ^{19}F spectra are referenced to TMS and $CFCl_3$, respectively and they were fitted by using the DMFit software [22]. ^{19}F

solid state NMR was used to quantify the fluorine content on the $TiOF_2$ samples by using reference samples [7-9]. ^{19}F solid-state MAS NMR (Hahn echo) spectra were also recorded for YF_3 and LaF_3 and the masses of each sample in the rotor were measured. The fits of the spectra allow to determine the integrated intensities (I) for each sample. Since, for each sample, the recycle delays were chosen to ensure that the amount of signal detected is maximum (420 s for YF_3 and 120 s for LaF_3), we assume that the integrated intensities are proportional to the number of scans (256 for the $TiOF_2$ samples and 16 for YF_3 and LaF_3) and to the molar quantity of fluorine atoms (n) in the rotor. This assumption is verified since the calculated I/n ratio for YF_3 and LaF_3 are equal. The intensities per scan of the NMR signals of the $TiOF_2$ samples, I_1, and of YF_3 (or LaF_3), I_2, allow to calculate the fluorine wt. % in the $TiOF_2$ samples using the following formula where m and M are the mass and the molar mass, respectively:

$$\frac{I_1}{I_2} = \frac{n_{F(TiOF_2)}}{\frac{3m_{YF_3}}{M_{YF_3}}}$$

$$F\ wt.\% = \frac{m_{F(TiOF_2)}}{m_{TiOF_2}} = \frac{n_{F(TiOF_2)}M_F}{m_{TiOF_2}} = \frac{3m_{YF_3}}{M_{YF_3}}\frac{I_1}{I_2}\frac{M_F}{m_{TiOF_2}}$$

Electrochemical characterization.

Electrodes were prepared by hand-milling of active material (80 wt. %), acetylene black (10 wt. %) as conductive agent and polyvinylidene difluoride (10 wt. %) previously dissolved in N-methyl-2-pyrrolidone (NMP, Sigma-Aldrich) as the binder. The resulting paste was coated onto a copper foil using a doctor blade. The electrode was dried in an oven at 75 °C overnight to evaporate NMP solvent and then cut into chips with a diameter of 1 cm and a typical mass of active material of 2 mg. The chips were outgassed in a vacuum furnace at 110 °C overnight and stored inside a glove box under argon atmosphere for battery assembly. The electrochemical characterization *vs.* lithium was carried out in a lithium metal half-cell. A solution of $LiPF_6$ dissolved in EC/DMC (LP30, Merck) was used as the electrolyte. The cells were tested in the voltage range of 1.2-3.0 V using a current density of 26.3 $mA.g^{-1}$. The used current density corresponds to a 0.1 C rate referring to the 263 $mAh.g^{-1}$ theoretical capacity of $TiOF_2$ based on the reaction of one mol of Li in 10 hours.

Results and discussion

The x-ray diffraction pattern of the as-prepared compound can be fully indexed using a cubic cell characteristic of $TiOF_2$ (space group Pm-3m). The lattice parameter was refined to 3.8076(1) Å, which is close to that reported by Vorres and Donohue, that is 3.798(5) Å [23]. The fluoride content was quantified by ^{19}F solid state NMR as described in the experimental section. The fluorine wt. % is 32.3 which is slightly lower than expected for pure $TiOF_2$, *i.e.* 37.3 wt. %. Such a difference accounts for a deviation of the oxydifluoride composition emphasizing the presence of OH groups. The latter was quantified using TGA. The TG curve **(Figure 1)** shows a continuous weight loss of 6.88 wt. % from 140 to 350 °C, characteristic of OH groups departure in water form ($2\ OH^- \rightarrow O^{2-} + H_2O$). It should be noted that beyond 350-400 °C, gaseous TiF_4 can form yielding an oxide phase having the anatase type structure [10].

X-ray diffraction analysis performed on the powder recovered after the TGA shows the presence of a small amount of anatase TiO_2 indicating that the dehydroxylation reaction has occurred yielding anionic partitioning. Assuming that both F^- and O^{2-} can be substituted by OH^-, the substitution of O^{2-} yields a negative charge deficiency counterbalanced by the creation of titanium vacancies. The general composition of hydroxylated $TiOF_2$ can then be written as $Ti_{1-x}\square_xO_{1-4x}(OH)_{4x+y}F_{2-y}$, where $\square$ represents a titanium vacancy. Based on ^{19}F solid state NMR and TG analyses, the following composition $Ti_{0.90}\square_{0.10}O_{0.60}(OH)_{0.74}F_{1.66}$ was established. The decomposition path can be summarized as follows:

$$Ti_{0.90}\square_{0.10}O_{0.60}(OH)_{0.74}F_{1.66} \rightarrow 0.83\cdot TiOF_2 + 0.07\cdot TiO_2 + 0.37\ H_2O$$

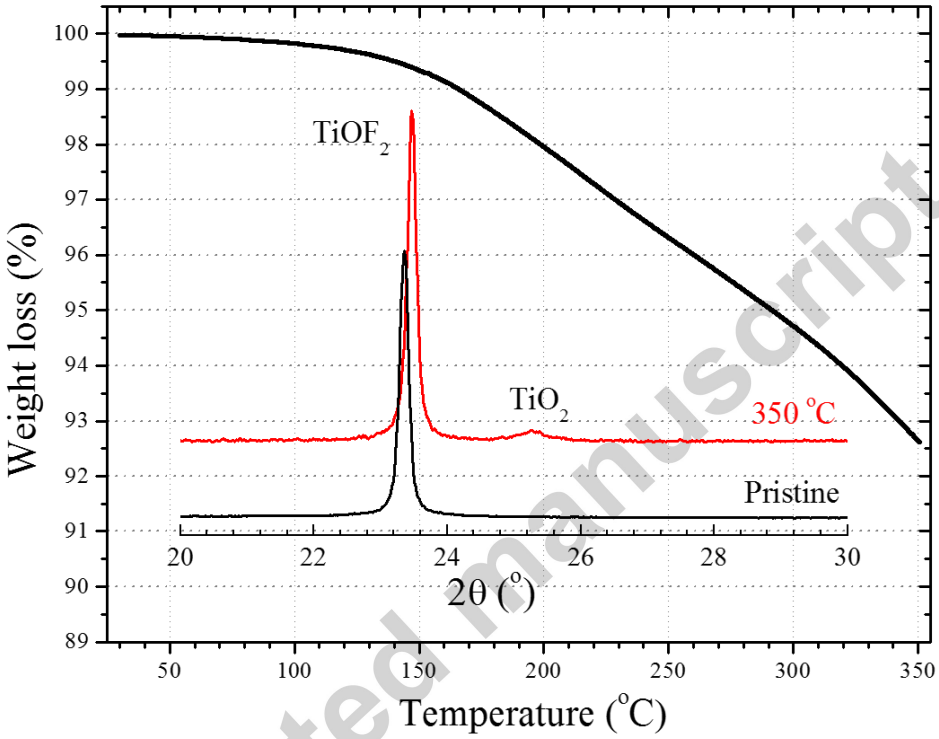

Figure 1. Thermogravimetric analysis performed under He. Inset: XRD patterns of the sample before and after TGA analysis.

The local environments of the fluorine atoms were investigated by ^{19}F solid state MAS NMR **(Figure 2)**. The spectrum was reconstructed using four lines located at ~ 12, 20, 146 and 182 ppm (Table 1) emphasizing different types of local environments for the F atoms. Within pure $TiOF_2$, an anion is surrounded by two titanium atoms. The occurrence of titanium vacancies induces additional coordination modes for the anions. Assuming random distributions of vacancies and Ti on the (1a) titanium and of O, F and OH on the (3d) anionic Wyckoff sites, the probabilities of occurrence of the various anionic environments are 81 % for Ti-X-Ti, 18 % for Ti-X-$\square$ and 1 % for $\square$-X-$\square$ (where X = O, F or OH). The last case can obviously be ruled out leading to probabilities of occurrence equal to 80 % for Ti-X-Ti and 20% for Ti-X-$\square$. The main lines (relative intensities equal to 82%) located at ~ 12 and 20.3 ppm are assigned to bridging fluorine atoms Ti-F-Ti. The lines located at higher chemical shift values, *i.e.* ~ 146 and 182 ppm (relative intensities equal to 18%), are assigned to fluorine atoms close to titanium vacancies Ti-F-$\square$. These assignments are in agreement with the increase of the

chemical shift of the anion when the number of surrounding cations decreases, as observed for ^{19}F NMR in NbF_5 and TaF_5 [24] and in the anatase $Ti_{0.78}\square_{0.22}O_{1.12}(OH)_{0.48}F_{0.40}$ [7] and for ^{17}O NMR in TiO_2(B) [25]. The ^{19}F δ_{iso} values of the fluorine atoms close to titanium vacancies Ti-F-$\square$ are significantly larger than those measured for F-Ti$\square_2$ in the anatase $Ti_{0.78}\square_{0.22}O_{1.12}(OH)_{0.48}F_{0.40}$ (98 ppm [7]) and for terminal F in K_2TiF_6 (71.4 ppm [26]) and in hybrid hydroxyfluorotitanates (IV) (76 to 82 ppm [27]). This may be due to shorter F-Ti bond lengths for these fluorine atoms in $Ti_{0.90}\square_{0.10}O_{0.60}(OH)_{0.74}F_{1.66}$ [28,29]. Broad ^{19}F NMR lines are observed, especially for the fluorine atoms close to titanium vacancies Ti-F-$\square$, in relation with the strong local disorder due to the occurrence of vacancies on the titanium site and the occupancy of the anionic site by three different anions. F-Ti bond lengths are then widely distributed, especially for the fluorine atoms close to titanium vacancies Ti-F-$\square$. The similar values of probabilities of occurrence of the Ti-X-Ti and for Ti-X-$\square$ environments and of relative intensities of the ^{19}F NMR resonances assigned to Ti-F-Ti and for Ti-F-$\square$ environments pointed out that fluorine atoms are uniformly distributed around titanium atoms and vacancies. Then, assuming that oxygen atoms preferentially bridges two titanium atoms, it suggests that OH groups are preferentially located close to vacancies (*i.e.* more than expected assuming random distributions).

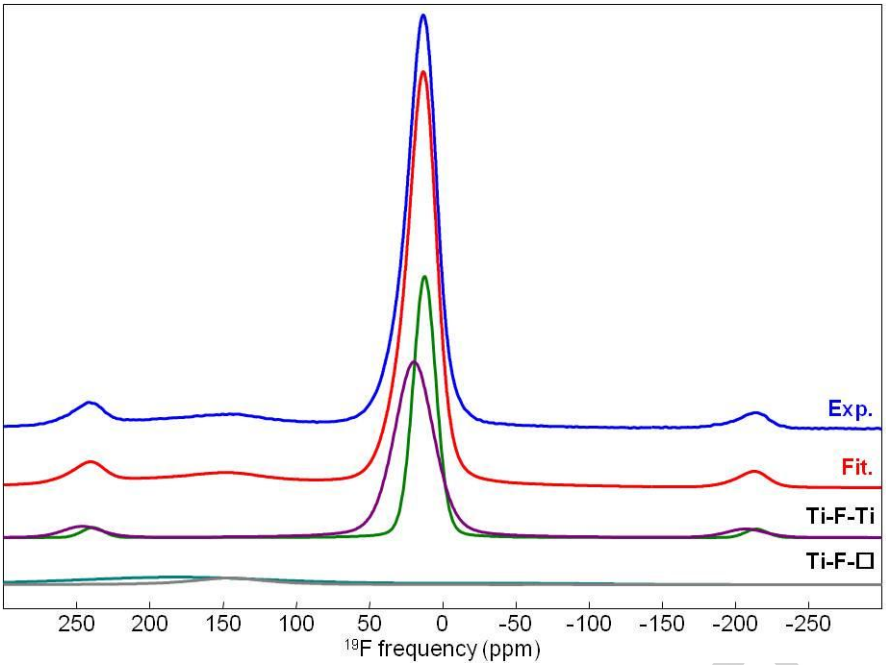

Figure 2. Experimental (blue) and fitted (red) ^{19}F MAS (64 kHz) NMR spectra of $Ti_{0.90}\square_{0.10}O_{0.60}(OH)_{0.74}F_{1.66}$. The individual resonances used for the fit and assigned to Ti-F-Ti and Ti-F-□ environments are shown below.

Table 1. Isotropic chemical shifts (δ_{iso}, ppm), line widths (LW, ppm), and relative intensities (I, %) of the NMR resonances used for the fit of the ^{19}F MAS (64 kHz) NMR spectrum of $Ti_{0.90}\square_{0.10}O_{0.60}(OH)_{0.74}F_{1.66}$ and assignment of these NMR resonances.

δ_{iso}	LW	I	Assignment
12.2	18.2	35.6	Ti-F-Ti
19.5	31.5	45.9	Ti-F-Ti
145.6	60.4	14.4	Ti-F-□
182.2	167.3	4.1	Ti-F-□

^{1}H solid-state MAS NMR offers a direct insight into the local environment of the hydrogen atoms in the structure of $Ti_{0.90}\square_{0.10}O_{0.60}(OH)_{0.74}F_{1.66}$. The spectrum (**Figure 3)** was fitted with two rather narrow signals at ~ 0.9 and 1.3 ppm and four broader signals at ~1.6, 6.7, 8.5 and 10.1 ppm (Table 2). In the case of anatase, signals observed at chemical shifts equal to 2.3 and 6.7 ppm have been assigned to terminal and bridging OH groups, respectively [30]. The signals with the largest δ_{iso} values could then be tentatively assigned to the more acidic OH groups coordinated to two Ti atoms, Ti-OH-Ti, while the signals with the smallest δ_{iso} values more likely belong to the more basic OH groups coordinated to one Ti atom, Ti-OH-□. However, it is well established that the ^{1}H chemical shift of a hydrogen-bonded proton is a very sensitive indicator of the strength of that hydrogen-bonding interaction (the strongest the

hydrogen-bonding interaction, the highest the chemical shift) related to the O-H...O distance [31,32]. Hydrogen bonding interactions O-H...O(F) of various strengths due to various O-H...O(F) distances, in relation with the strong local disorder, may be responsible for the quite large ranges of δ_{iso} values of each kind of OH groups. Moreover, it cannot be excluded that hydrogen bonded Ti-OH-□ and non or weakly hydrogen bonded Ti-OH-Ti may have similar chemical shifts (Table 2). In any event, Ti-OH-□ account for at least 30 % confirming that OH groups are preferentially located close to vacancies (*i.e.* more than expected assuming random distributions).

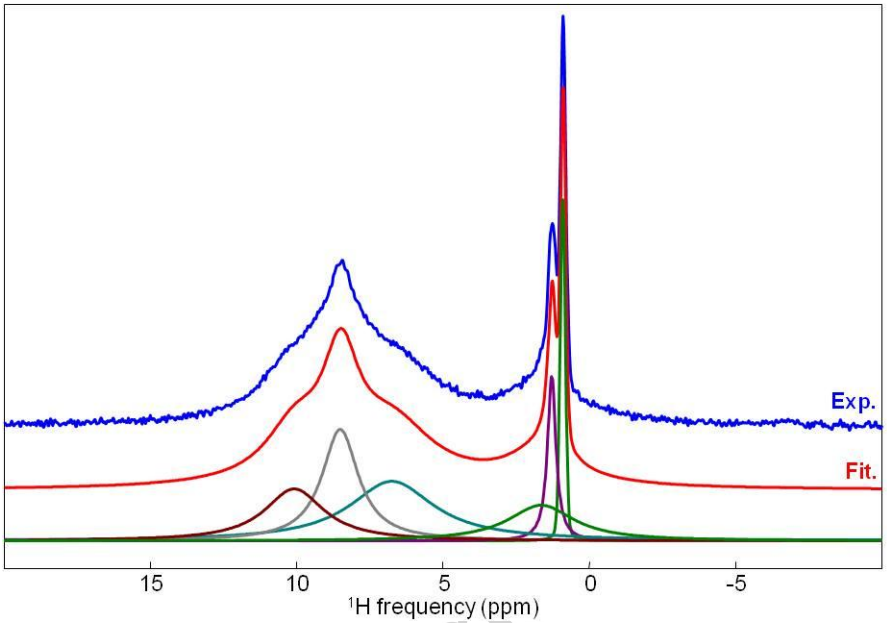

Figure 3. Experimental (blue) and fitted (red) ^{1}H MAS (44 kHz) NMR spectra of $Ti_{0.90}\square_{0.10}O_{0.60}(OH)_{0.74}F_{1.66}$. The individual resonances used for the fit are shown below.

Table 2. Isotropic chemical shifts (δ_{iso}, ppm), line widths (LW, ppm) and relative intensities (I, %) of the NMR resonances used for the reconstruction of the ^{1}H MAS (44 kHz) NMR spectrum of $Ti_{0.90}\square_{0.10}O_{0.60}(OH)_{0.74}F_{1.66}$ and tentative assignment of these NMR resonances .

δ_{iso}	LW	I	Assignment
0.90	0.21	7.9	Ti-OH-□
1.27	0.35	8.4	Ti-OH-□
1.64	2.75	13.4	Ti-OH-□
6.74	3.48	28.2	Ti-OH-Ti (and H-bonded Ti-OH-□)
8.50	1.50	24.1	Ti-OH-Ti
10.1	2.46	17.9	Ti-OH-Ti

In order to investigate its thermal behavior, $Ti_{0.90}\square_{0.10}O_{0.60}(OH)_{0.74}F_{1.66}$ was treated at different temperatures, *i.e.* 150, 170, 200 and 300 °C, and further characterized by means of

XRD and solid state NMR spectroscopy. According to X-ray diffraction analysis **(Figure 4)**, single phases of cubic-like $TiOF_2$ were obtained up to 170 °C. Thereafter, a peak appears at 25.3° (2θ) corresponding to the (110) plan of TiO_2 anatase (space group $I4_1/amd$).

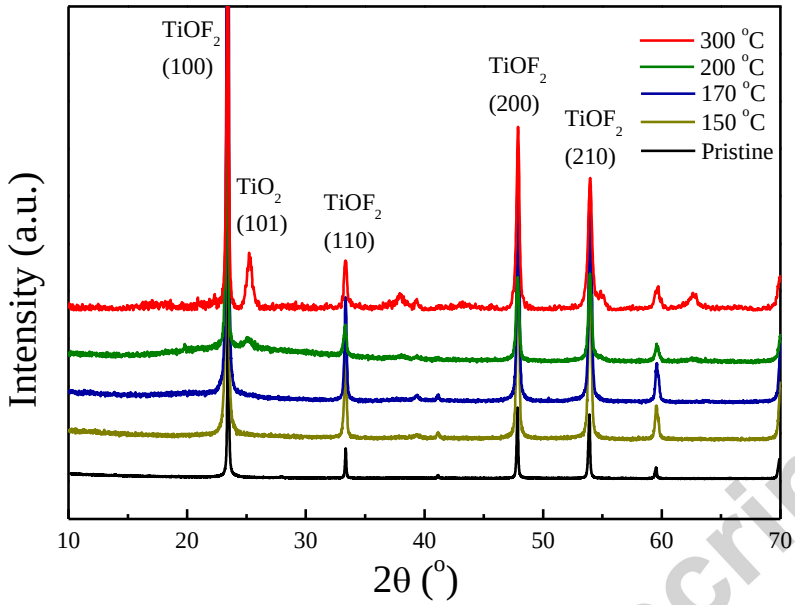

Figure 4. X-ray diffraction patterns of $Ti_{0.90}\square_{0.10}O_{0.60}(OH)_{0.74}F_{1.66}$ before and after thermal treatments. The temperatures of the thermal treatments are indicated.

Figure 5 shows the ^{19}F MAS NMR spectra of $Ti_{0.90}\square_{0.10}O_{0.60}(OH)_{0.74}F_{1.66}$ before and after thermal treatments. The fits of the spectra of $Ti_{0.90}\square_{0.10}O_{0.60}(OH)_{0.74}F_{1.66}$ after thermal treatments are given as Supplementary data (Fig. S1-S4, Tables S1-S4). In the single phase region, *i.e.* T ≤ 170 °C, the relative intensities of the resonances located at higher chemical shift values, assigned to Ti-F-□, decrease (from ~ 18 % to 10 %) confirming the dehydroxylation of the framework which is further corroborated by a slight increase of the fluorine content to 33-34 wt %. At higher temperature, *i.e.* T = 200 and 300 °C, the relative intensity of the resonance assigned to Ti-F-□ continue to decrease (~ 6.5 % for T = 200°C) and finally this resonance vanishes for T = 300 °C. The appearance of the TiO_2 anatase phase is concomitant with a significant decrease of the fluorine wt % down to ca. 20 %. Such a decrease is due to hydrolysis of the framework and the departure of gaseous TiF_4. A new resonance located at ca. – 88 ppm appears which is characteristic of fluorine atoms surrounded by three titanium atoms, *i.e.* F-Ti_3, as in the anatase $Ti_{0.78}\square_{0.22}O_{1.12}(OH)_{0.48}F_{0.40}$ [7]. The substitution of O^{2-} by F^- in anatase TiO_2 yields a negative charge deficiency counterbalanced by the creation of titanium vacancies. The expected Ti_2-F-□ (-5 ppm [7]) environments are probably hidden by the resonances of the Ti-F-Ti environments of the main phase on the ^{19}F MAS NMR spectrum. However, the occurrence of Ti-F-$\square_2$ environments (98 ppm [7]) in the anatase present in the sample after thermal treatment at 300°C is not evidenced on the ^{19}F MAS NMR spectrum showing that the titanium vacancy and fluorine rates are small. Finally, this shows that the use of $TiOF_2$ as a precursor for the formation of TiO_2 anatase can yield to samples containing fluorine and titanium vacancies.

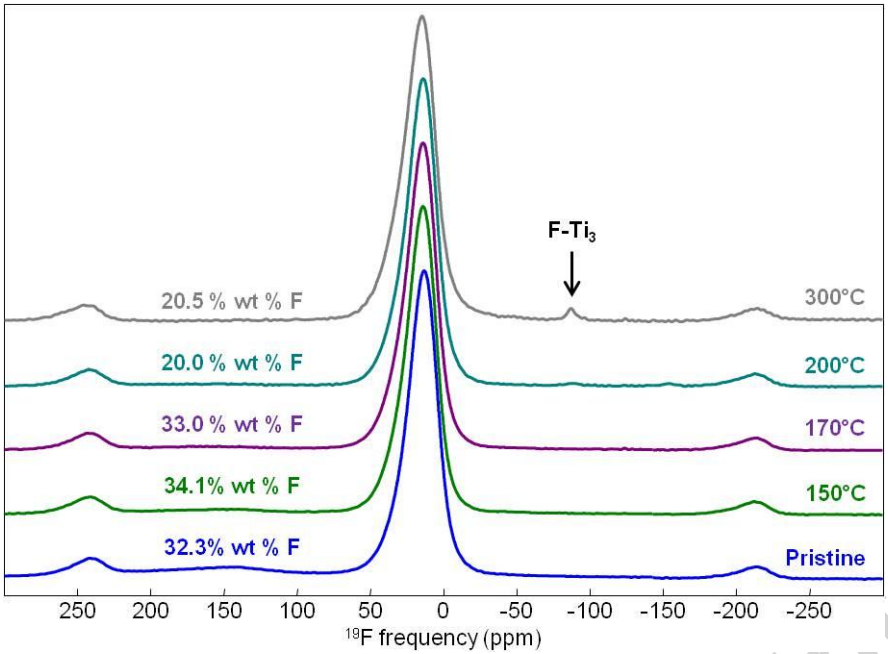

Figure 5. ^{19}F MAS (64 kHz) NMR spectra of $Ti_{0.90}\square_{0.10}O_{0.60}(OH)_{0.74}F_{1.66}$ before and after thermal treatments. Spectra are normalized to the most intense peak. The fluorine wt % and the temperatures of the thermal treatments are indicated. The arrow indicates F-Ti_3 environments.

Figure 6 shows the ^{1}H MAS NMR spectra before and after thermal treatments. As expected, when the temperature of the thermal treatment increases, the quantity of OH groups decreases but does not vanish (approximately reduced by a factor of 3 for 200 °C and 300 °C). The fits of the spectra of $Ti_{0.90}\square_{0.10}O_{0.60}(OH)_{0.74}F_{1.66}$ after thermal treatments are given as Supplementary data (Fig. S6-S9, Tables S5-S8). When the temperature of the thermal treatment increases, the NMR resonances with the smallest chemical shifts (assigned to OH groups from Ti-OH-□ in the pristine) broaden and overlap with the NMR resonances having the largest chemical shifts (assigned to OH groups from Ti-OH-Ti in the pristine). Assignment of the NMR resonances used for the fits of the spectra to OH groups from Ti-OH-Ti or Ti-OH-□ solely is then meaningless. When the temperature of thermal treatment increases, the averaged and weighted chemical shift decreases from 6.2 ppm for the pristine to 3.8 ppm for 170 °C and hereafter remains roughly constant. It may be due to a decrease of the strength of the hydrogen bonding interactions and/or to an increase of the ratio of OH groups from Ti-OH-□.

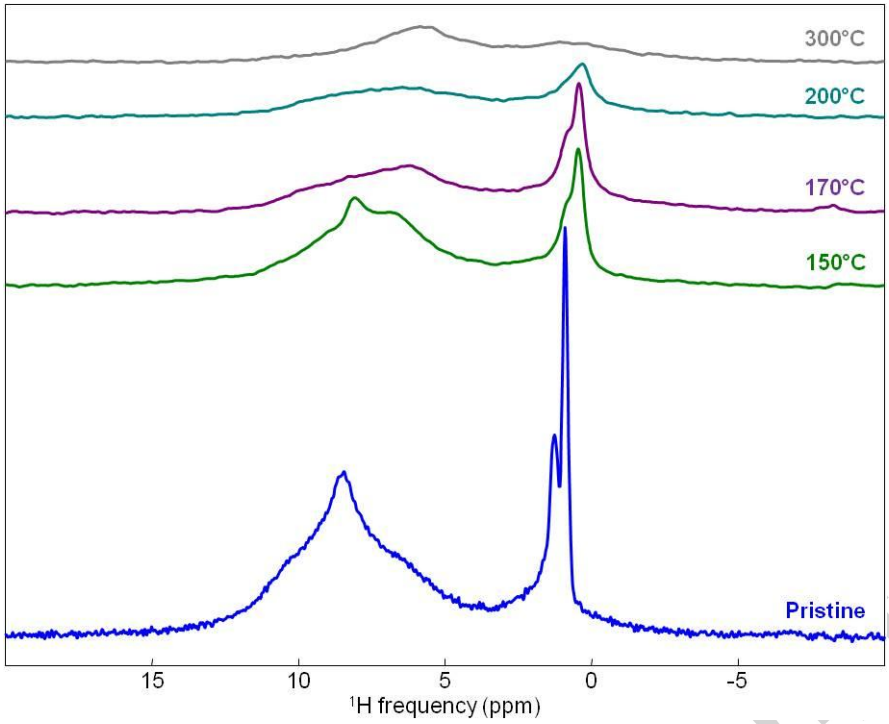

Figure 6. ^{1}H MAS (44 kHz) NMR spectra of $Ti_{0.90}\square_{0.10}O_{0.60}(OH)_{0.74}F_{1.66}$ before and after thermal treatments. The temperatures of the thermal treatments are indicated. The number of scans (16) is the same for these five spectra and the masses of sample in the rotor are equal to 3.6, 3.1, 3.2, 3.4 and 2.4 mg for pristine and samples treated at 150°C, 170°C, 200°C and 300°C, respectively. Spectra normalized to the most intense peak are given as Supplementary data (Fig. S5).

The electrochemical properties of compounds related to $TiOF_2$ largely depend on the preparation method. A literature overview of the electrochemistry of compounds related to $TiOF_2$ pointed out different electrochemical behaviors vs. lithium in the intercalation region, *i.e.* 1.2-3.4 V. **Table 3** compares the different electrochemical properties along with the synthesis method employed. Two main routes can be distinguished: (i) gas phase fluorination and (ii) solution based processes. Fluorination of titanium dioxide using elemental fluorine enable to prepare pure oxyfluoride compounds free of OH groups [15,16] whereas solution-based methods more likely favor the stabilization of OH groups within $TiOF_2$ [9,10]. The presence of OH groups depends on the synthesis parameters (nature of the precursor, heating mode, concentration of the reactants, etc) and particularly on the medium used, *i.e.* aqueous medium very likely favors the stabilization of OH groups. Although the presence of OH groups was not systematically discussed in the literature, thermal analyses can indicate their presence [12,17]. Moreover, from the **Table 3**, a trend can be observed: the higher the OH content, the lower the first discharge capacity. It is particularly well exemplified when comparing the lithium uptake in the hydroxyfluoride $Ti_{0.75}\square_{0.25}F_{1.5}(OH)_{1.5}$ [10] and $TiOF_2$ obtained by fluorination of TiO_2 using elemental fluorine [15] that are 0.17 and 0.84 Li^+ per formula unit, respectively. Protons of OH groups likely localize close to the interstitial site prone to accommodate lithium in the ReO_3 type structure thus blocking lithium intercalation. Such a steric effect has been postulated to occur in $LiTiOF_2$ containing protons, *i.e.* $Li_xH_yTiOF_2$, prepared by chemical lithiation [17].

Table 3. Synthesis methods, presence of OH groups and electrochemical properties of $TiOF_2$ based compounds.

Synthesis method	Observations	First discharge capacity / voltage cutoff / current density	References
Ti metal treated with $HF:HNO_3$	Likely contains OH groups	~ 100 $mAh.g^{-1}$/1V/30 $mA.g^{-1}$	[11]
Microwave synthesis in aqueous medium	$Ti_{0.75}\square_{0.25}F_{1.5}(OH)_{1.5}$	~ 50 $mAh.g^{-1}$/1V/100 $mA.g^{-1}$	[12]
Solvothermal synthesis – hydrolysis of TiF_4 in non-aqueous medium	Absence of OH groups based on FTIR data	~ 160 $mAh.g^{-1}$/1V/400 $mA.g^{-1}$	[13]
Solvothermal synthesis	No traces of OH groups based on TGA analysis	~ 200 $mAh.g^{-1}$/1V/30 $mA.g^{-1}$	[14]
Gas phase fluorination of TiO_2 anatase	Free of OH groups	~ 145 $mAh.g^{-1}$/1.2V/ 26.3 $mA.g^{-1}$ ~ 220 $mAh.g^{-1}$/1.2V/ 2.63 $mA.g^{-1}$	[15]
Gas phase fluorinations of TiO_2 and TiN_xO_y	Two samples free of OH: O-$TiOF_2$ N-$TiOF_2$	~ 116 $mAh.g^{-1}$/1V/ 33.5 $mA.g^{-1}$ ~ 330 $mAh.g^{-1}$/1V/ 33.5 $mA.g^{-1}$	[16]
Solvothermal synthese Hexagonal-$TiOF_2$ cubic-$TiOF_2$	h-$TiOF_2$: no OH groups c-$TiOF_2$: OH groups based on TGA analysis	~ 215 $mAh.g^{-1}$/1V/ 33.5 $mA.g^{-1}$ ~ 230 $mAh.g^{-1}$/1V/ 33.5 $mA.g^{-1}$	[17]

To confirm the blocking effect of OH groups, the intercalation of lithium was investigated on samples containing different contents of OH groups, *i.e.* the pristine $Ti_{0.90}\square_{0.10}O_{0.60}(OH)_{0.74}F_{1.66}$ and compounds dehydroxylated at 150 and 170 °C. **Figure 7** shows the first discharge/charge curves obtained for Li half cells cycled between 1.2 and 3.4 V at C/10 (C refers to 263 $mAh.g^{-1}$: the theoretical capacity of $TiOF_2$ based on the intercalation of 1 Li^+ per formula unit). During the first cycle, $Ti_{0.90}\square_{0.10}O_{0.60}(OH)_{0.74}F_{1.66}$ can accommodate 0.43 Li^+ (*ca.* 115 $mAh.g^{-1}$) and further charges only 0.19 Li^+ (*ca.* 50 $mAh.g^{-1}$). The partial deshydroxylation of the structure by thermal treatments notably improves the lithiation/de-lithiation with the highest reversibility obtained after the thermal treatment at 170 °C. This result tends to support the blocking effect of OH groups on the electrochemical properties *vs.* Li^+/Li. Moreover, the dehydroxylation increases the lithium insertion voltage suggesting that the reaction is more favorable. A similar trend was previously observed [17]: a cubic $TiOF_2$ containing OH groups shows a lower insertion potential than the hexagonal polymorph free of OH. Nevertheless, the remaining OH groups in the sample thermally treated at 170 °C still prevent higher lithiation degree to be obtained.

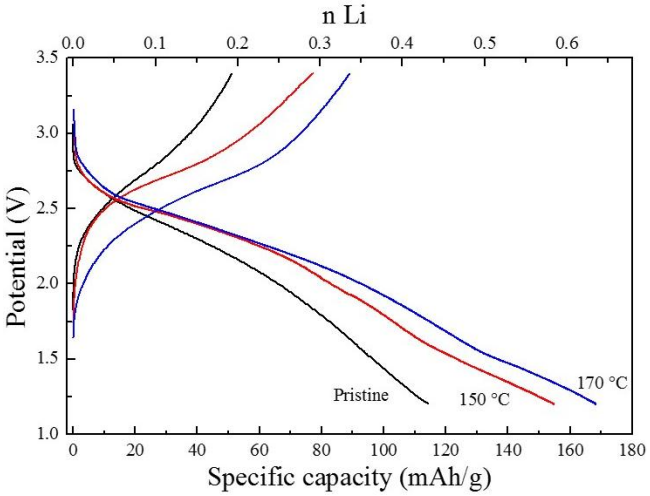

Figure 7. First discharge/charge curves for the pristine $Ti_{0.90}\square_{0.10}O_{0.60}(OH)_{0.74}F_{1.66}$ and partially deshydroxylated compounds at 150 and 170 °C.

Conclusion

In this work, we prepared hydroxylated $TiOF_2$ based compound using a solvothermal synthesis assisted by microwave heating. The resulting compound featured OH groups substituting the oxide/fluoride sublattice resulting in the stabilisation of titanium vacancies which has been rationalized by the following general chemical formula $Ti_{1-x}\square_xO_{1-4x}(OH)_{4x+y}F_{2-y}$. While their presence was quantified by thermal analysis, ^{1}H NMR provided spectroscopic signatures assigned to Ti-OH-□ and Ti-OH-Ti species. Moreover, ^{19}F NMR allowed to identify Ti-F-□ and Ti-F-Ti species further supporting the presence of titanium vacancies. Finally, investigating the intercalation properties of hydroxylated and $TiOF_2$ based compounds revealed that OH groups prevent the insertion of lithium within the interstitial sites of the ReO_3 type structure demonstrating that an accurate determination of the chemical composition is required to understand the physico-chemical properties of electrode materials.

Acknowledgments

The research leading to these results has received funding from the People Programme (Marie Curie Actions) of the European Union's Seventh Framework Programme (FP7/2007-2013) under REA grant agreement n°[321879] (FLUOSYNES). Alain Demourgues and Madhu Channabasappa (ICMCB-CNRS) are gratefully acknowledged for access and help with the microwave apparatus.

References

[1] S. Rüdiger, E. Kemnitz, The fluorolytic sol–gel route to metal fluorides—a versatile process opening a variety of application fields, Dalton Trans. (2008) 1117–1127. doi:10.1039/B716483A.

[2] A. Demourgues, N. Penin, D. Dambournet, R. Clarenc, A. Tressaud, E. Durand, About MX_3 and MX_2 (M^{n+} = Mg^{2+}, Al^{3+}, Ti^{4+}, Fe^{3+}; X^{p-} = F^-, O^{2-}, OH^-) nanofluorides, J. Fluorine Chem. 134 (2012) 35–43. doi:10.1016/j.jfluchem.2011.02.006.

[3] M. Leblanc, V. Maisonneuve, A. Tressaud, Crystal Chemistry and Selected Physical Properties of Inorganic Fluorides and Oxide-Fluorides, Chem. Rev. 115 (2015) 1191–1254. doi:10.1021/cr500173c.

[4] J. H. Moss, A. Wright, Titanium(IV) oxydifluoride, J. Fluorine Chem. 5 (1975) 163–167. doi:10.1016/S0022-1139(00)81702-9.
[5] K. Dehnicke, Syntheses of Oxide Halides, Angew. Chem. Int. Ed. Engl. 4 (1965) 22–29. doi:10.1002/anie.196500221.
[6] A. P. Wilkinson, R. E. Josefsberg, L. C. Gallington, C. R. Morelock, C. M. Monaco, History-dependent thermal expansion in NbO_2F, J. Solid State Chem. 213 (2014) 38–42. doi:10.1016/j.jssc.2014.02.003.
[7] W. Li, D. Corradini, M. Body, C. Legein, M. Salanne, J. Ma, et al., High Substitution Rate in TiO_2 Anatase Nanoparticles with Titanium Vacancies for Fast Lithium Storage, Chem. Mater. 27 (2015) 5014–5019. doi:10.1021/acs.chemmater.5b01407.
[8] W. Li, M. Body, C. Legein, O.J. Borkiewicz, D. Dambournet, Atomic Insights into Nanoparticle Formation of Hydroxyfluorinated Anatase Featuring Titanium Vacancies, Inorg. Chem. 55 (2016) 7182–7187. doi:10.1021/acs.inorgchem.6b01259.
[9] W. Li, M. Body, C. Legein, D. Dambournet, Sol–Gel Chemistry of Titanium Alkoxide toward HF: Impacts of Reaction Parameters, Crystal Growth & Design. 16 (2016) 5441–5447. doi:10.1021/acs.cgd.6b00910.
[10] A. Demourgues, N. Penin, E. Durand, F. Weill, D. Dambournet, N. Viadere, A. Tressaud, New Titanium Hydroxyfluoride $Ti_{0.75}(OH)_{1.5}F_{1.5}$ as a UV Absorber, Chem. Mater. 21 (2009) 1275–1283. doi:10.1021/cm8030297.
[11] M. V. Reddy, S. Madhavi, G. V. Subba Rao, B. V. R. Chowdari, Metal oxyfluorides $TiOF_2$ and NbO_2F as anodes for Li-ion batteries, J. Power Sources 162 (2006) 1312–1321. doi:10.1016/j.jpowsour.2006.08.020.
[12] D. Dambournet, K. W. Chapman, P. J. Chupas, R. E. Gerald, N. Penin, C. Labrugere, A. Demourgues, A. Tressaud, K. Amine, Dual Lithium Insertion and Conversion Mechanisms in a Titanium-Based Mixed-Anion Nanocomposite, J. Am. Chem. Soc. 133 (2011) 13240–13243. doi:10.1021/ja204284h.
[13] Y. Zeng, W. Zhang, C. Xu, N. Xiao, Y. Huang, D. Y. W. Yu, H. H. Hng, Q. Yan, One-Step Solvothermal Synthesis of Single-Crystalline $TiOF_2$ Nanotubes with High Lithium-Ion Battery Performance, Chem. Eur. J. 18 (2012) 4026–4030. doi:10.1002/chem.201103879.
[14] L. Chen, L. Shen, P. Nie, X. Zhang, H. Li, Facile hydrothermal synthesis of single crystalline $TiOF_2$ nanocubes and their phase transitions to TiO_2 hollow nanocages as anode materials for lithium-ion battery, Electrochimica Acta. 62 (2012) 408–415. doi:10.1016/j.electacta.2011.12.058.
[15] N. Louvain, Z. Karkar, M. El-Ghozzi, P. Bonnet, K. Guérin, P. Willmann, Fluorination of anatase TiO_2 towards titanium oxyfluoride $TiOF_2$: a novel synthesis approach and proof of the Li-insertion mechanism, J. Mater. Chem. A. 2 (2014) 15308–15315. doi:10.1039/C4TA02553A.
[16] J. M. Powell, J. Adcock, S. Dai, G. M. Veith, C. A. Bridges, Role of precursor chemistry in the direct fluorination to form titanium based conversion anodes for lithium ion batteries, RSC Adv. 5 (2015) 88876–88885. doi:10.1039/C5RA17258F.
[17] B. Li, D. Wang, Y. Wang, B. Zhu, Z. Gao, Q. Hao, Y. Wang, K. Tang, One-step synthesis of hexagonal $TiOF_2$ as high rate electrode material for lithium-ion batteries: research on Li intercalation/de-intercalation mechanism, Electrochimica Acta. 180 (2015) 894–901. doi:10.1016/j.electacta.2015.09.034.
[18] X. Rocquefelte, F. Goubin, Y. Montardi, N. Viadere, A. Demourgues, A. Tressaud, M.-H. Whangbo, S. Jobic, Analysis of the Refractive Indices of TiO_2, $TiOF_2$, and TiF_4: Concept of Optical Channel as a Guide To Understand and Design Optical Materials, Inorg. Chem. 44 (2005) 3589–3593. doi:10.1021/ic048259w.
[19] C. Z. Wen, Q. H. Hu, Y. N. Guo, X. Q. Gong, S. Z. Qiao, H. G. Yang, From titanium oxydifluoride ($TiOF_2$) to titania (TiO_2): phase transition and non-metal doping with enhanced photocatalytic hydrogen (H_2) evolution properties, Chem. Commun. 47 (2011) 6138–6140.
[20] Z. Huang, Z. Wang, K. Lv, Y. Zheng, K. Deng, Transformation of $TiOF_2$ Cube to a Hollow Nanobox Assembly from Anatase TiO_2 Nanosheets with Exposed {001} Facets via Solvothermal Strategy, ACS Appl. Mater. Interfaces 5 (2013) 8663−8669.
[21] J. Wang, F. Cao, Z. Bian, M. K. H. Leung, H. Li, Ultrafine single-crystal $TiOF_2$ nanocubes with mesoporous structure, high activity and durability in visible light driven photocatalysis, Nanoscale 6 (2014) 897−902.
[22] D. Massiot, F. Fayon, M. Capron, I. King, S. Le Calvé, B. Alonso, J.-O. Durand, B. Bujoli, Z. Gan, G. Hoatson, Magn. Reson. Chem. 40 (2002) 70−76.
[23] K. Vorres, J. Donohue, The structure of titanium oxydifluoride, Acta Crystallogr. 8 (1955) 25–26. doi:10.1107/S0365110X55000054.
[24] M. Biswal, M. Body, C. Legein, A. Sadoc, F. Boucher, NbF_5 and TaF_5: Assignment of ^{19}F NMR resonances and chemical bond analysis from GIPAW calculations, J. Solid State Chem. 207 (2013) 208–217.
[25] Y. Ren, Z. Liu, F. Pourpoint, A. R. Armstrong, C. P. Grey, P. G. Bruce, Nanoparticulate TiO_2(B): An Anode for Lithium-Ion Batteries, Angew. Chem. Int. Ed. 51 (2012) 2164-2167.

[26] C. J. L. Silwood, I. Abrahams, D. C. Apperley, N. P. Lockyer, E. Lynch, M. Motevalli, R. M. Nix, M. Grootveld, Surface analysis of novel hydroxyapatite bioceramics containing titanium(IV) and fluoride, J. Mater. Chem. 15 (2005) 15, 1626-1636.
[27] J. Lhoste, M. Body, C. Legein, A. Ribaud, M. Leblanc, V. Maisonneuve, F^-/OH^- substitution in $[H_4tren]^{4+}$ and $[H_3tren]^{3+}$ hydroxyfluorotitanates(IV) and classification of tren cation configurations, J. Solid State Chem. 2014, 217, 72-79.
[28] B. Bureau, G. Silly, J.-Y. Buzaré, J. Emery, Chem. Phys. 249 (1999) 89–104.
[29] M. Body, G. Silly, C. Legein, J.-Y. Buzaré, Inorg. Chem. 43 (2004) 2474–2485.
[30] M. Crocker, R. H. M. Herold, A. E. Wilson, M. Mackay, C. A. Emeis, A. M. Hoogendoorn, J. Chem. Soc., Faraday Trans. 92 (1996) 2791–2798.
[31] R. K. Harris, P. Jackson, L. H. Merwin, B. J. Say, G. Hagele, J. Chem. Soc., Faraday Trans. 84 (1988) 3649–3672.
[32] H. Eckert, J. P. Yesinowski, L. A. Silver, E. M. Stolper, J. Phys. Chem., 1988, 92, 2055–2064.

Highlights

- Evidences of the presence of OH groups and titanium vacancies in titanium oxyfluoride.
- ^1H NMR showed the presence of Ti-OH-Ti and Ti-OH-□ species.
- The presence of OH groups limits the insertion of lithium within the interstitial sites.